



Low-Cost and Biodegradable Thermoelectric Devices Based on van der Waals Semiconductors on Paper Substrates

Gulsum Ersu , Carmen Munuera, Federico J. Mompean, Daniel Vaquero, Jorge Quereda, João Elias F. S. Rodrigues, Jose A. Alonso, Eduardo Flores, Jose R. Ares, Isabel J. Ferrer, Abdullah M. Al-Enizi, Ayman Nafady, Sruthi Kuriakose, Joshua O. Island*, and Andres Castellanos-Gomez* 

We present a method to fabricate handcrafted thermoelectric devices on standard office paper substrates. The devices are based on thin films of WS₂, Te, and BP (P-type semiconductors) and TiS₃ and TiS₂ (N-type semiconductors), deposited by simply rubbing powder of these materials against paper. The thermoelectric properties of these semiconducting films revealed maximum Seebeck coefficients of $(+1.32 \pm 0.27)$ mV K⁻¹ and (-0.82 ± 0.15) mV K⁻¹ for WS₂ and TiS₃, respectively. Additionally, Peltier elements were fabricated by interconnecting the P- and N-type films with graphite electrodes. A thermopower value up to 6.11 mV K⁻¹ was obtained when the Peltier element were constructed with three junctions. The findings of this work show proof-of-concept devices to illustrate the potential application of semiconducting van der Waals materials in future thermoelectric power generation as well as temperature sensing for low-cost disposable electronic devices.

1. Introduction


Industry and wider society are pushing toward the integration of electronic functionalities into every mundane gadget, commonly referred to as ubiquitous electronics.^[1,2] Several widespread electronics applications like wearables, smart tags/patches, and point-of-care devices demand the development of ultra-low-cost and disposable electronic components.^[3,4] Disposable silicon-supported devices may lead to a significant electronic waste problem as only a small fraction of them can be recycled.^[5,6] Paper has emerged as a promising substrate material for disposable electronic applications due to its ultra-low-cost (10 000 times cheaper than crystalline silicon) and biodegradability.^[7–10] Moreover, its hypoallergenic character makes it particularly suitable for biomedical

applications where disposable devices are preferred to avoid contagious outbreaks.^[11–13]

Several paper-supported devices with different functionalities (e.g. thermistors, gas sensors, strain gauges, field-effect transistors, and photodetectors) have been reported to date.^[14–27] However, there is still great opportunity for improving the strategies to power up these devices. There is a massive global interest catered toward improved energy storage applications like supercapacitors and solar cells that can be easily fabricated and are cost-effective. The recent technique of hand-drawn electrodes on paper substrates using pencils has opened the door to paper-supported energy storage.^[28–30] These paper-based energy storage solutions are paving the way for “green” and sustainable devices to meet the ever-increasing demand for power. Using simple hand-drawn techniques, paper-based supercapacitors have been realized with high areal capacitances of 2.3 mF cm⁻² along with long-term cycling stability.^[30] Biodegradable bacteria-powered batteries on paper substrates have also emerged as a green solution for ubiquitous electronics.^[31,32] Harnessing light for solar energy, organic solar cells with power conversion efficiencies up to 13% have been achieved using paper substrates.^[33,34]

Thermoelectric-based power generators have the potential to scavenge heat waste (such as body temperature) to operate low-power consumption devices.^[35–37] Paper-based thermoelectric devices offer the opportunity to confirm the devices to a range of surfaces without compromising its performance; related examples have been reported

G. Ersu, Dr. C. Munuera, Dr. F. J. Mompean, Dr. J. E. F. S. Rodrigues, Prof. J. A. Alonso, Dr. S. Kuriakose, Dr. A. Castellanos-Gomez
Materials Science Factory, Instituto de Ciencia de Materiales de Madrid (ICMM-CSIC), Madrid E-28049, Spain
E-mail: andres.castellanos@csic.es
D. Vaquero
Nanotechnology Group, USAL–Nanolab, Univesidad de Salamanca, Salamanca Junta de Castilla y León 37007, Spain
Dr. J. Quereda
GISC, Departamento de Física de Materiales, Universidad Complutense de Madrid, Madrid E-28040, Spain
Dr. E. Flores
Departamento de Física Aplicada, Centro de Investigación y Estudios Avanzados, Mérida 97310, Mexico
Dr. J. R. Ares, Prof. I. J. Ferrer
MIRE Group, Departamento de Física de Materiales, Universidad Autónoma de Madrid, Madrid E-28049, Spain
Prof. I. J. Ferrer
Instituto Nicolás Cabrera, Universidad Autónoma de Madrid, Madrid E-28049, Spain
Prof. A. M. Al-Enizi, Prof. A. Nafady
Department of Chemistry, College of Science, King Saud University, Riyadh 11451, Saudi Arabia
Dr. J. O. Island
Department of Physics and Astronomy, University of Nevada Las Vegas, Las Vegas NV 89154, USA
E-mail: joshua.island@unlv.edu

 The ORCID identification number(s) for the author(s) of this article can be found under <https://doi.org/10.1002/eem2.12488>.

DOI: 10.1002/eem2.12488

recently.^[38–40] Among these endeavors, pencil-drawn graphite thermoelectric generators on paper substrates produced Seebeck coefficients of $16 \mu\text{V K}^{-1}$ and open-circuit voltages of 9 mV at 60 K temperature differentials.^[38,39] Recent devices with sputter-coated copper iodide and bismuth have reached open-circuit voltages of 84.5 mV at a 50 °C temperature differential.^[40] Paper-supported thermoelectric devices can also find applications in temperature sensing and photodetectors based on the thermopile operation principle.^[41] While these preliminary studies

are promising, improvements in device characteristics may come via the incorporation of van der Waals materials with intrinsic P- and N-type character.

Herein, thermoelectric devices on standard copy paper with semiconducting van der Waals materials have been fabricated using tungsten disulfide (WS_2), tellurium (Te), and black phosphorus (BP) as P-type materials and titanium trisulfide (TiS_3) and titanium disulfide (TiS_2) as N-type materials. Notably, WS_2 has the largest P-type Seebeck coefficient of $+1.32 \pm 0.27 \text{ mV K}^{-1}$, whereas TiS_3 results in the highest N-type Seebeck coefficient of $-0.82 \pm 0.15 \text{ mV K}^{-1}$. Thus, from these two materials we constructed a series of thermoelectric generators with 1, 2, and 3 P–N junctions. For each addition of a series junction, our recorded thermoelectric voltage increases, reaching a maximum value of 120 mV at a temperature difference of 22.3 °C.

2. Results and Discussion

The semiconducting van der Waals materials are deposited onto standard (untreated) copy paper by abrasion-induced deposition as described elsewhere but we detail the fabrication of P–N junctions using a masking technique here.^[42–44] Figure 1 shows an example of our fabrication process for a 3-junction Peltier module consisting of WS_2 (P-type) and TiS_3 (N-type). A vinyl-cutter (Portrait Silhouette) is used to fabricate a stencil mask to deposit the P- and N-type materials. Figure 1a illustrates a typical example of a vinyl mask placed on the surface of a piece of standard copy paper. Pieces of low-tack Nitto SPV224 tape are placed on the mask openings ($25 \text{ mm} \times 5 \text{ mm}$) designed for the N-type semiconductor while the P-type counterpart is being deposited. The different semiconductors are then deposited by rubbing powder of the selected van der Waals material against the unmasked regions of the paper substrate with a cotton swab. Using this method results in films that are approximately $20 \mu\text{m}$ thick. Figure 1b–f show how the P-type material, WS_2 , is deposited on the surface followed by deposition of the N-type material, TiS_3 . Following this, we use a soft graphite pencil (Cretacolor Monolith 9B, 204 09) to draw electrodes on the ends of the semiconducting rectangles (Figure 1g). The stencil mask is then removed leaving well-defined semiconducting rectangles (alternating WS_2 and TiS_3) with graphite leads at their ends (Figure 1h). Finally, the graphite electrodes are connected to form several junctions of N- and P-type materials to form Peltier modules in series (Figures 1i,j). See Figures S1 and S2, Supporting Information and Zhang et al.^[44] for scanning electron microscopy characterization of the different van der Waals materials films on paper.

The performance of the fabricated devices is characterized by a homebuilt probe station with two probes supplemented with spring-loaded tips for the electrical connections and two probes with thermocouples to measure the temperature difference across the measured devices. The sample stage consists of two commercially available Peltier modules (TEC1-12706) side-by-side to apply a temperature gradient across the sample. Figure 2a shows a picture of a thermoelectric device consisting of three Peltier modules in series, formed by 3 P–N junctions, tested in our homebuilt probe station. Figure 2b displays a thermal camera image of the same device, where the difference in temperature between the two sides of the device is evident. Note that, due to the difference in emissivity of the different materials, the thermal image is not quantitative, and an accurate temperature difference measurement has to be carried out with the thermocouple probes. The thermocouple probe accuracy (100 mK) gives a precise measurement of

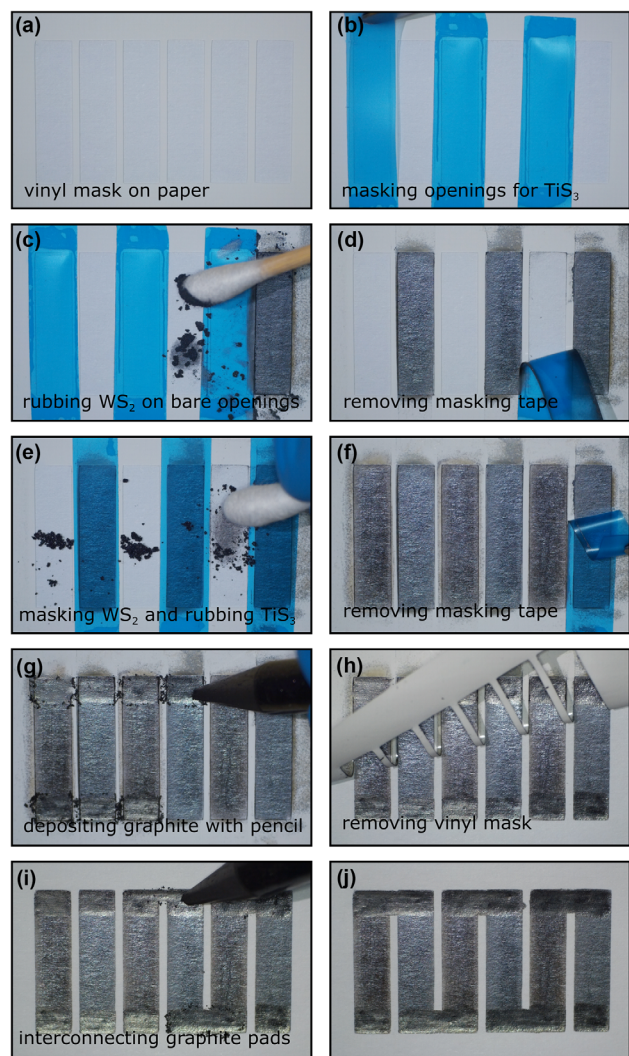


Figure 1. Fabrication of handcrafted Peltier elements on paper. a) A vinyl mask is placed onto the surface of the paper with rectangular openings where the semiconducting material will be deposited. b) The openings where the N-type material (TiS_3) will be deposited are first masked with Nitto SPV224 tape. c) The P-type material (WS_2) is deposited on the paper surface by rubbing micronized WS_2 powder. d) The Nitto tape mask is removed. e) The WS_2 films are masked with Nitto tape, and TiS_3 is deposited on the unmasked paper by rubbing TiS_3 powder. f) The Nitto tape mask is removed. g) Graphite pads are deposited at the edges of the semiconducting rectangular films with an 9B pencil. h) The vinyl mask is removed. i) The graphite pads are interconnected with 9B pencil to create the series of junctions between the P- and N-type materials. j) Picture of the completed device after fabrication.

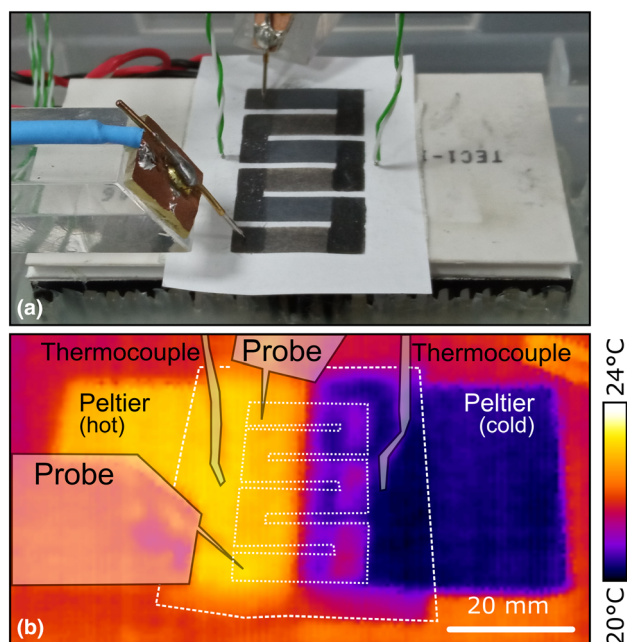


Figure 2. Apparatus for testing thermoelectric devices on paper. a) Picture of the experimental setup used to characterize the thermoelectric performance of the fabricated devices. A homebuilt probe station is used to make electrical connection to the graphite pads, and two probe arms are supplemented with thermocouples that are used to measure the temperature difference across the device. Two commercial Peltier elements are used to control the temperature difference across the device. b) Thermal camera image of the device under study when the two Peltier elements are biased to have an approximately 4 °C temperature difference.

the temperature of the Peltier modules. Also, as shown in the qualitative thermal camera image (Figure 2 and Figure S3, Supporting Information) the Peltier elements produce a homogeneous temperature across the surface contributing to the accuracy of the measurements.

We begin with the thermoelectric properties of the individual semiconducting van der Waals materials. Figure 3a shows current versus voltage (IV hereafter) characteristics of a WS₂ film on paper with graphite electrodes (see the inset for a picture of the device) for various temperature differences between the cold side and the hot side. Upon temperature difference increase the slope of the IVs increases, as expected for a semiconducting material with thermally activated conductivity,^[43] and the open-circuit voltage (i.e. the voltage at which $I = 0$) progressively shifts away from zero. Note that these measurements are performed with double sweeps to look for any hysteresis and voltage shifts. Unlike in other studies where the thermoelectric voltage shift is directly measured with a voltmeter, we extract this value from linear fits to current versus voltage characteristics that provides a higher degree of accuracy in its determination and avoids systematic uncertainties due to offsets in the electronic measurement setups. The voltage shift (V_{th}) is due to the thermoelectric effect:

$$V_{th} = -S(T_h - T_c) \quad (1)$$

where S is the Seebeck coefficient of the WS₂ film and T_h and T_c are the temperature of the hot and cold sides. We determined that

the contribution of the metal probes and graphite pads to the measured thermopower is lower than 20 $\mu\text{V K}^{-1}$ (Figure S4, Supporting Information).

Figure 3b plots the built-in thermoelectric voltage (ΔV) as a function of the temperature difference ($T_h - T_c = \Delta T$). The dataset follows a linear trend, and its slope gives a direct measurement of the Seebeck coefficient of the WS₂ film on paper. For this WS₂ film, we record a Seebeck coefficient of +1.09 mV K^{-1} , indicating hole majority carriers (P-type). This is roughly four times larger than the Seebeck coefficient obtained from polycrystalline WS₂ pressed pellets ($\approx 0.25 \text{ mV K}^{-1}$)^[45] and is likely a result of the large surface to volume ratio of the film on paper device and its ability to hold a higher temperature difference when compared with bulk counterparts.^[46] In the films, the heat must dissipate through the substrate/air interface which is less efficient when compared with bulk counterparts. Figure 3c,d illustrates the same characterization as in Figure 3a,b but now for a TiS₃ film on paper. For this TiS₃ film, we obtain a Seebeck coefficient of -1.01 mV K^{-1} , indicating electron majority carriers (N-type). This is also larger than the value obtained from bulk pressed pellets of TiS₃ ($\approx 0.625 \text{ mV K}^{-1}$).^[47,48] Although we do not fully understand the origin of the improvement in the WS₂ and TiS₃ film over bulk pellets, we believe that it may arise from a difference in their density of charge carriers. While in the pressed pellets, the WS₂ and TiS₃ flakes are surrounded by other flakes of similar dielectric constant, the porous structure of the films on paper ensures that the flakes are more exposed to atmospheric adsorbates that can affect the doping level of the flakes. Detailed characterizations of the thermoelectric properties of films of Te, BP (from two different sources), BP (3% Ge), and TiS₂ on paper are provided in the Supporting Information.

Table 1 summarizes the obtained results on the single-material films (see Figures S5–S8, Supporting Information). Among all studied materials, WS₂ gives rise to the largest P-type Seebeck coefficient of $(1.32 \pm 0.27) \text{ mV K}^{-1}$ for 21 fabricated devices, whereas TiS₃ produces the greatest N-type Seebeck coefficient of $(-0.82 \pm 0.15) \text{ mV K}^{-1}$ among 17 tested devices. It is noteworthy to mention that slightly different Seebeck coefficients are measured for BP from two different sources and growth methods. In this regard, our in-house BP, grown by high-pressure synthesis, yields a larger Seebeck coefficient, whereas the BP sourced from Smart Elements is based on the vapor transport method. Moreover, we further studied a second batch of BP samples in-house with 3% of Ge added to the growth capsule. While the compositional and structural characterization showed us that a negligible amount of Ge was included in the structure, we measured a huge increase in the Seebeck coefficient (more than a factor of 2) of the material in comparison to the pristine BP. Due to the environmental degradation of BP upon atmospheric exposure,^[49] we decided to employ WS₂ as a P-type semiconductor for the fabrication of the Peltier modules to ensure their stability and reproducibility. Statistical analysis of all the films revealed that the variation in the measured Seebeck coefficient roughly scales with the magnitude of the obtained values. A thorough characterization of the electrical resistivity of these films, another important parameter to assess the performance of these materials in thermoelectric applications, can be found in full detail in Zhang et al.^[44] Briefly, films of WS₂ show resistivity values in the 70–370 $\Omega\cdot\text{m}$ range and TiS₃ $\sim 4 \Omega\cdot\text{m}$. See Figure S9, Supporting Information for the resistivity estimation for Te and BP (3% Ge) films on paper that were not reported in Zhang et al.^[44]

The thermoelectric properties of the fabricated devices using a series of junctions between WS₂ and TiS₃ are characterized in

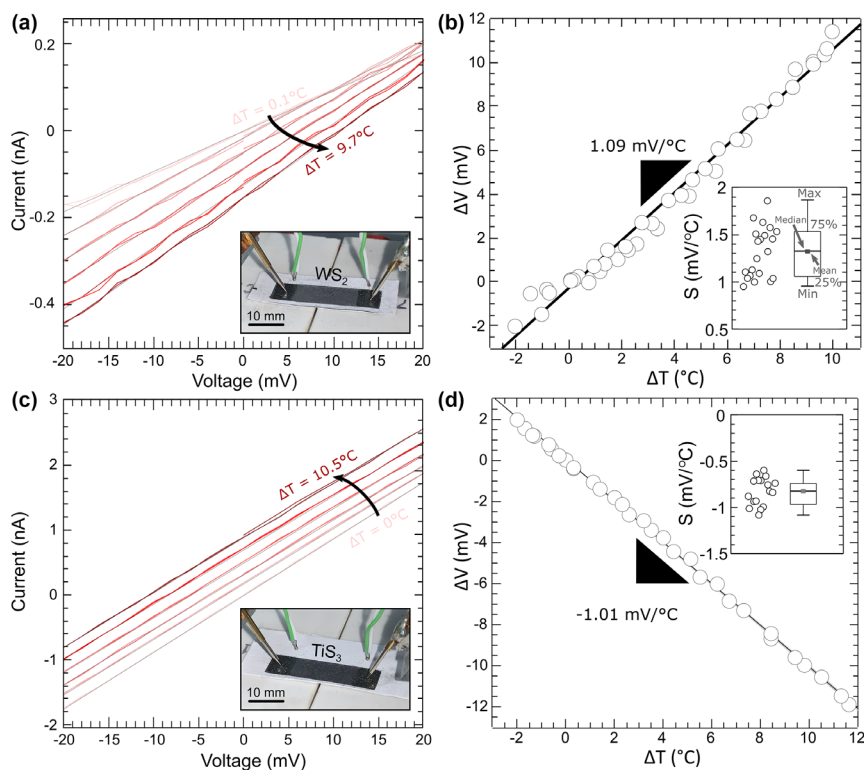


Figure 3. Characterization of the thermoelectric performance of WS_2 and TiS_3 films. a) Current versus voltage characteristics (IVs) of a WS_2 film with graphite electrode pads at different temperature differences (ΔT). Upon increase of ΔT , the IVs increase their slope and shift toward higher voltage values developing a voltage offset (ΔV). These sweeps are doubled to look for any hysteresis or voltage shifts. The inset shows a picture of the device measured. b) ΔV as a function of ΔT , measured in the WS_2 film for several temperature difference cycles. The slope of the dataset provides a direct measurement of the Seebeck coefficient of the WS_2 film. The inset shows a box plot representation of the Seebeck coefficient measured on 21 WS_2 films. c) IVs of a TiS_3 film at different ΔT showing a shift toward negative voltages upon increase of ΔT . These sweeps are doubled to look for any hysteresis or voltage shifts. The inset shows a picture of the device measured. d) ΔV as a function of ΔT , measured in the TiS_3 film for several temperature difference cycles. The inset shows a box plot representation of the Seebeck coefficient measured on 17 TiS_3 films.

Table 1. Summary of the thermoelectric property statistics for single material films. Seven materials are presented with the number of devices measured, the median Seebeck coefficient value, the standard deviation, and the median two-terminal resistance.

Material	# Devices	Median S (mV K^{-1})	Standard deviation (mV K^{-1})
WS_2	21	1.3	0.3
Te	6	0.48	0.05
BP (smart elements)	6	0.43	0.04
BP (in-house)	6	0.56	0.04
BP (in-house, 3% Ge)	6	1.4	0.4
TiS_3	17	-0.82	0.15
TiS_2	6	-0.28	0.02

Figure 4. Figure 4a shows the built-in voltage measured for a thermoelectric device formed with 1, 2, and 3 P-N junctions in series as a function of the temperature difference between the two ends of the device. The three datasets follow linear trends whose slopes provide the thermopower of the Peltier element formed by those junctions. As expected, the thermopower scales with the number of P-N junctions connected in series, reaching a remarkable value of 6.11 mV K^{-1} . This is significantly larger than very recent, multi-junction copper iodide/bismuth thermoelectric devices on cellulose paper (1.69 mV K^{-1})^[40] and graphite-derived thermoelectric generators on paper (0.15 mV K^{-1}).^[39] Additionally, Figure 4b displays two IVs measured on the thermoelectric generator formed with 3 P-N junctions when the temperature difference between the two ends is negligible (black) and 22.3°C (red). At a temperature difference of 22.3°C , an open circuit voltage of $V_{\text{OC}} = 120 \text{ mV}$ and a short circuit current of $I_{\text{SC}} = 0.2 \text{ nA}$ are recorded. The maximum output power for a thermoelectric generator can be estimated from $P = I_{\text{SC}}V_{\text{OC}}/4$, which assumes a linear relationship between the generated voltage and current as well as an impedance-matched load.^[40,46,50] For the fabricated three junction device, an output power of 6 pW was measured. In comparison, thermoelectric devices created with sputtered films produce output powers of 215 nW .^[40] The output power is moderately low and reflects the high internal resistances of our thin-film thermoelectric generator (from the slope in Figure 4b, we estimate that the resistance of the device is in the $1 \text{ G}\Omega$ range). Improvements in output power could be achieved with optimization of thin film deposition and granular

structure; both topics are the focus of future research. The large thermopower values obtained from these proof-of-concept devices, however, can be considered in very appealing applications such as temperature sensing (for biophysical sensors e.g.) or infrared photodetection where the generation of large open-circuit voltages is highly desired.

3. Conclusion

In conclusion, we have presented the thermoelectric properties of abrasion-deposited thin films on paper and multi-junction thermoelectric generators. Out of the seven tested materials, WS_2 , Te, BP (Smart Elements), BP (in-house), BP (in-house with 3% Ge), TiS_2 , and TiS_3 , the highest P-type Seebeck coefficients, and the highest N-type coefficient have been accomplished using WS_2 and TiS_3 , respectively. Using these two materials, we fabricated and reported the characteristics of 1,

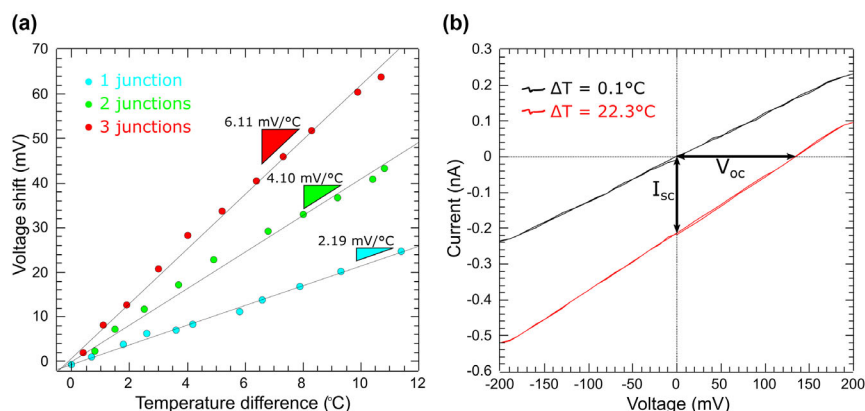


Figure 4. Characterization of the thermoelectric performance of a Peltier element with 1, 2, and 3 junctions. a) Voltage shift as a function of the temperature difference across the devices for Peltier elements formed with 1, 2, and 3 junctions. The slope of the different datasets provides a direct measurement of their thermopower values that is nearly proportional to the number of junctions forming the Peltier element. b) I/Vs of a Peltier element with 3 junctions with a negligible temperature difference across the device (black) and with an approximately 22 °C temperature difference (red). The device presents current flow, even in unbiased conditions, of ~ -0.2 nA (called short circuit current, I_{sc}), and it develops a voltage shift (called open-circuit voltage V_{oc}) of approximately 120 mV.

2, and 3 P–N junction thermoelectric generators. A remarkably high output voltage of 120 mV for the three-junction device was recorded at a temperature difference of 22.3 °C. The findings of this work highlight the promising use of van der Waals materials on paper for applications in low-cost, biodegradable thermoelectric devices.

4. Materials and Methods

Tungsten disulfide (WS_2) micronized powder was purchased from Hagen Automation Ltd.

TiS_2 (PN: 12826.06) high purity powder purchased from Alfa Aesar.

TiS_3 powders were synthesized by a solid–gas reaction of metal powders of Ti (Goodfellow, 99.5%) with sulfur (Merck, 99.75%) at molar ratios of $M/S = 3$ in a vacuum-sealed ampoule annealed at 550 °C for 60 h.^[51]

In-house black phosphorus (BP) was prepared via a high-pressure procedure in a piston–cylinder press (Rockland Research Co.), and a pressure of 2 GPa at a high temperature of 1073 K for 1 h. At the start, tiny pieces of amorphous red phosphorus (Alfa-Aesar) were ground in an agate mortar inside a nitrogen-filled glove box; the material was sealed in a niobium capsule and then placed inside a cylindrical graphite heater. After quenching and releasing pressure, pieces of BP (6–7 mm in diameter; 5 mm in thickness) were recovered.^[52] The as-prepared BP chunks were crushed and manually ground in an agate mortar before abrasion-induced deposition on paper. A second set of BP samples were synthesized in-house but adding a 3% of Ge to the capsule. Structural and chemical composition characterization shows that Ge was not incorporated into the lattice within the experimental uncertainty. We thus believe that a very small presence of Ge could be acting as a diluted dopant within the BP crystals.

Commercially available black phosphorus (Smart Elements) and Tellurium (Novaelements) high purity (>99.99%) chunks were crushed and manually ground in an agate mortar before abrasion-induced deposition on paper.

Acknowledgements

This work was funded by the European Research Council (ERC) under the European Union's Horizon 2020 research and innovation program (grant agreement

no. 755655, ERC-StG 2017 project 2D-TOPSENSE), the Ministry of Science and Innovation (Spain) through the project PID2020-115566RB-I00. A.M.A. and A.N. extend their sincere appreciation to the Distinguished Scientist Fellowship Program (DSFP) at King Saud University for partial funding of this work. J.Q. acknowledge financial support from the Agencia Estatal de Investigación de Spain (Grants PID2019-106820RB, RTI2018-097180-B-I00, and PGC2018-097018-B-I00) and the Junta de Castilla y León (Grants SA256P18 and SA121P20), including funding by ERDF/FEDER. J.Q. acknowledges financial support from Universidad Complutense de Madrid and European Commission (MSCA COFUND UNA4CA-REER grant. Project number 4129252). J.Q. acknowledges financial support from MICINN (Spain) through the program Juan de la Cierva-Incorporación. J.A.A. thanks the financial support of the Spanish Ministry of Industry and Competitiveness to the project MAT2017-84496-R. J.R.A. and I.J.F. acknowledge financial support from the Ministry of Science and Innovation (Spain) through the project RT2018-099794-B-I00. D.V. acknowledges financial support from the Ministry de Universities (Spain) (Ph.D. contract FPU19/04224).

Conflict of Interest

The authors declare no conflict of interest.

Supporting Information

Supporting Information is available from the Wiley Online Library or from the author.

Keywords

paper-based electronics, Seebeck effect, semiconductors, thermoelectrics, van der Waals materials

Received: June 6, 2022

Revised: July 4, 2022

Published online: July 17, 2022

- [1] S. R. Forrest, *Nature* **2004**, 428, 911.
- [2] A. Nathan, A. Ahnood, M. T. Cole, Sungsik Lee, Y. Suzuki, P. Hiralal, F. Bonaccorso, T. Hasan, L. Garcia-Gancedo, A. Dyadyusha, S. Haque, P. Andrew, S. Hofmann, J. Moultrie, D. Chu, A. J. Flewitt, A. C. Ferrari, M. J. Kelly, J. Robertson, G. A. J. Amaratunga, W. I. Milne, *Proc. IEEE* **2012**, 100, 1486.
- [3] V. Selamneni, A. BS, P. Sahatiya, *Med. DEVICES Sens.* **2020**, 3, e10099.
- [4] A. Quddious, S. Yang, M. Khan, F. Tahir, A. Shamim, K. Salama, H. Cheema, *Sensors* **2016**, 16, 2073.
- [5] V. Forti, C. P. Baldé, R. Kuehr, G. Bel, *Global E-waste Monitor* **2020**.
- [6] S. Nandy, S. Goswami, A. Marques, D. Gaspar, P. Grey, I. Cunha, D. Nunes, A. Pimentel, R. Igreja, P. Barquinha, L. Pereira, E. Fortunato, R. Martins, *Adv. Mater. Technol.* **2021**, 6, 2000994.
- [7] A. Russo, B. Y. Ahn, J. J. Adams, E. B. Duoss, J. T. Bernhard, J. A. Lewis, *Adv. Mater.* **2011**, 23, 3426.
- [8] F. Eder, H. Klauk, M. Halik, U. Zschieschang, G. Schmid, C. Dehm, *Appl. Phys. Lett.* **2004**, 84, 2673.
- [9] D. Tobjörk, R. Österbacka, *Adv. Mater.* **2011**, 23, 1935.

- [10] Y. Xu, G. Zhao, L. Zhu, Q. Fei, Z. Zhang, Z. Chen, F. An, Y. Chen, Y. Ling, P. Guo, S. Ding, G. Huang, P. Y. Chen, Q. Cao, Z. Yan, *Proc. Natl. Acad. Sci. USA* **2020**, 117, 18292.
- [11] J. K. F. Lee, *J. Paediatr. Child Health* **2008**, 44, 62.
- [12] D. W. Eyre, A. E. Sheppard, H. Madder, I. Moir, R. Moroney, T. P. Quan, D. Griffiths, S. George, L. Butcher, M. Morgan, R. Newnham, M. Sunderland, T. Clarke, D. Foster, P. Hoffman, A. M. Borman, E. M. Johnson, G. Moore, C. S. Brown, A. S. Walker, T. E. A. Peto, D. W. Crook, K. J. M. Jeffery, *N. Engl. J. Med.* **2018**, 379, 1322.
- [13] J. J. Weems, *Infect. Control Hosp. Epidemiol.* **1993**, 14, 583.
- [14] T.-K. Kang, *Appl. Phys. Lett.* **2014**, 104, 073117.
- [15] T. Dinh, H. P. Phan, D. V. Dao, P. Woodfield, A. Qamar, N. T. Nguyen, *J. Mater. Chem. C* **2015**, 3, 8776.
- [16] D.-J. Lee, D. Y. Kim, *IEEE Access* **2019**, 7, 77200.
- [17] C.-W. Lin, Z. Zhao, J. Kim, J. Huang, *Sci. Rep.* **2014**, 4, 3812.
- [18] N. Kurra, D. Dutta, G. U. Kulkarni, *Phys. Chem. Chem. Phys.* **2013**, 15, 8367.
- [19] H. Liu, H. Jiang, D. Zhang, Z. Li, H. Zhou, F. Du, *ACS Sustain. Chem. Eng.* **2017**, 5, 10538.
- [20] P. M. Pataniya, V. Patel, C. K. Sumesh, *Nanotechnology* **2021**, 32, 315709.
- [21] X. Liao, Z. Zhang, Q. Liao, Q. Liang, Y. Ou, M. Xu, M. Li, G. Zhang, Y. Zhang, *Nanoscale* **2016**, 8, 13025.
- [22] D. McManus, A. Dal Santo, P. B. Selvasundaram, R. Krupke, A. LiBassi, C. Casiraghi, *Flex. Print. Electron.* **2018**, 3, 034005.
- [23] B. Saha, S. Baek, J. Lee, *ACS Appl. Mater. Interfaces* **2017**, 9, 4658.
- [24] P. Pataniya, C. K. Zankat, M. Tannarana, C. K. Sumesh, S. Narayan, G. K. Solanki, K. D. Patel, V. M. Pathak, P. K. Jha, *ACS Appl. Nano Mater.* **2019**, 2, 2758.
- [25] K. A. Mirica, J. G. Weis, J. M. Schnorr, B. Esser, T. M. Swager, *Angew. Chem. Int. Ed.* **2012**, 51, 10740.
- [26] Y. Li, Y. A. Samad, T. Taha, G. Cai, S. Y. Fu, K. Liao, *ACS Sustain. Chem. Eng.* **2016**, 4, 4288.
- [27] H. Tai, Z. Duan, Y. Wang, S. Wang, Y. Jiang, *ACS Appl. Mater. Interfaces* **2020**, 12, 31037.
- [28] X. Zhang, Z. Lin, B. Chen, S. Sharma, C. P. Wong, W. Zhang, Y. Deng, *J. Mater. Chem. A* **2013**, 1, 5835.
- [29] M. P. Down, C. W. Foster, X. Ji, C. E. Banks, *RSC Adv.* **2016**, 6, 81130.
- [30] G. Zheng, L. Hu, H. Wu, X. Xie, Y. Cui, *Energy Environ. Sci.* **2011**, 4, 3368.
- [31] A. Fraiwan, S. Choi, *Phys. Chem. Chem. Phys.* **2014**, 16, 26288.
- [32] H. Lee, S. Choi, *Nano Energy* **2015**, 15, 549.
- [33] F. Brunetti, A. Operamolla, S. Castro-Hermosa, G. Lucarelli, V. Manca, G. M. Farinola, T. M. Brown, *Adv. Funct. Mater.* **2019**, 29, 1806798.
- [34] M. Rawat, E. Jayaraman, S. Balasubramanian, S. S. K. Iyer, *Adv. Mater. Technol.* **2019**, 4, 1900184.
- [35] F. J. DiSalvo, *Science* **1999**, 285, 703.
- [36] L. Habbe, J. Nurnus, *Electron. Cool.* **2011**, 17, 24.
- [37] Y. Du, K. Cai, S. Chen, H. Wang, S. Z. Shen, R. Donelson, T. Lin, *Sci. Rep.* **2015**, 5, 6411.
- [38] V. V. Brus, M. Gluba, J. Rappich, F. Lang, P. D. Maryanchuk, N. H. Nickel, *ACS Appl. Mater. Interfaces* **2018**, 10, 4737.
- [39] R. Mulla, D. R. Jones, C. W. Dunnill, *Adv. Mater. Technol.* **2020**, 5, 2000227.
- [40] R. Mulla, D. R. Jones, C. W. Dunnill, *Mater. Today Commun.* **2021**, 29, 102738.
- [41] A. L. Hsu, P. K. Herring, N. M. Gabor, S. Ha, Y. C. Shin, Y. Song, M. Chin, M. Dubey, A. P. Chandrakasan, J. Kong, P. Jarillo-Herrero, T. Palacios, *Nano Lett.* **2015**, 15, 7211.
- [42] A. Mazaheri, M. Lee, H. S. J. van der Zant, R. Frisenda, A. Castellanos-Gomez, *Nanoscale* **2020**, 12, 19068.
- [43] M. Lee, A. Mazaheri, H. S. J. van der Zant, R. Frisenda, A. Castellanos-Gomez, *Nanoscale* **2020**, 12, 22091.
- [44] W. Zhang, Q. Zhao, C. Munuera, M. Lee, E. Flores, J. E. F. Rodrigues, J. R. Ares, C. Sanchez, J. Gainza, H. S. J. van der Zant, J. A. Alonso, I. J. Ferrer, T. Wang, R. Frisenda, A. Castellanos-Gomez, *Appl. Mater. Today* **2021**, 23, 101012.
- [45] G. E. Yakovleva, A. I. Romanenko, A. S. Berdinsky, A. Y. Ledneva, V. A. Kuznetsov, M. K. Han, S. J. Kim, V. E. Fedorov, in *2016 39th Int. Convention on Information and Communication Technology, Electronics and Microelectronics (MIPRO)*, IEEE, Opatija, Croatia **2016**, pp. 5–9, <https://doi.org/10.1109/MIPRO.2016.7522100>.
- [46] N. Jaziri, A. Boughamou, J. Müller, B. Mezghani, F. Tounsi, M. Ismail, *Energy Rep.* **2020**, 6, 264.
- [47] P. R. N. Misse, D. Berthebaud, O. I. Lebedev, A. Maignan, E. Guilmeau, *Materials* **2015**, 8, 2514.
- [48] I. J. Ferrer, J. R. Ares, J. M. Clamagirand, M. Barawi, C. Sánchez, *Thin Solid Films* **2013**, 535, 398.
- [49] J. O. Island, G. A. Steele, H. S. J. van der Zant, A. Castellanos-Gomez, *2D Mater.* **2015**, 2, 011002.
- [50] P. Fan, Z. H. Zheng, Y. Z. Li, Q. Y. Lin, J. T. Luo, G. X. Liang, X. M. Cai, D. P. Zhang, F. Ye, *Appl. Phys. Lett.* **2015**, 106, 073901.
- [51] E. Flores, J. R. Ares, I. J. Ferrer, C. Sánchez, *Phys. Status Solidi RRL Rapid Res. Lett.* **2016**, 10, 802.
- [52] J. E. F. S. Rodrigues, J. Gainza, F. Serrano-Sánchez, C. López, O. J. Dura, N. Nemes, J. L. Martinez, Y. Huttel, F. Fauth, M. T. Fernández-Díaz, N. Biškup, J. A. Alonso, *Inorg. Chem.* **2020**, 59, 14932.